Negative Differential Resistance in Bidirectional Threshold Switching of Ag/HfOx/Pt Device

zhiguo jiang
Institute of Semiconductors ,South China Normal University
Dongliang Wang
Institute of Semiconductors ,South China Normal University
Yan Li
Institute of Semiconductors ,South China Normal University
Yong Zhang
Institute of Semiconductors ,South China Normal University
Xinman Chen (xmchenscnu@163.com)
South China Normal University

Nano Express

Keywords: Negative Differential Resistance, Threshold Switching, Conductive Filaments

Posted Date: February 17th, 2020

DOI: https://doi.org/10.21203/rs.2.23747/v1

Negative Differential Resistance in Bidirectional Threshold Switching of $Ag/HfO_x/Pt$ Device

Zhiguo Jiang [a], ***Dongliang Wang*** [a], ***Yan Li*** [a], ***Yong Zhang*** [a], ***Nasir Khisro*** [b], ***Xinman Chen*** [a,*]

[a] *Guangdong Engineering Research Center of Optoelectronic Functional Materials and Devices, Institute of Semiconductor Science and Technology, South China Normal University, Guangzhou 510631, China*

[b] *Physics Department, University of Kotli Azad Kashmir Pakistan, Azad Kashmir 11100, Pakistan*

Abstract

In this work, the dependence of negative differential resistance (NDR) on compliance current (I_{cc}) was investigated based on $Ag/HfO_x/Pt$ resistive memory device. Tunable conversion from bidirectional threshold switching (TS) to memory switching (MS) were achieved through enhancing I_{cc}. NDR can be observed in TS as I_{cc} is below 800μA but vanishes in MS. The switching voltages and readout windows of TS evolve with I_{cc}. Furthermore, the dynamic conductance (dI/dV) as a function of time in NDR can be well illustrated by capacitor-like relaxation equation, and the relaxation time constant is significantly dependent on I_{cc}. These phenomena were elucidated from viewpoint of nanofilament evolution controlled by I_{cc} as well as nanocapacitor effects originated from nanofilament gap. The I_{cc}-dependent NDR as well as conversion between TS and MS on $Ag/HfO_x/Pt$ resistive memory device indicates its potential application as a multifunctional electronic device.

Keywords:

RRAM, Negative Differential Resistance, Threshold Switching, Conductive Filaments.

* Author to whom correspondence should be addressed: xmchenscnu@163.com;

1. Introduction

Resistance random accessory memory (RRAM) based on the resistive switching (RS) phenomenon in capacitor-like metal-insulator-metal (MIM) devices has attracted significant attention due to its simple structure, easy fabrication, fast switching speed and superior scaling property.[1-3] Two basic switching modes were generally included according to the electrical switching behaviors of RRAM, namely memory switching (MS) and threshold switching (TS).[4-6] The MS is a kind of nonvolatile behavior, both high resistance state (HRS) and low resistance state (LRS) can be maintained after removing the external bias, enabling the application in the nonvolatile memories， reconfigurable logic and neuromorphic computing, which has been intensively investigated in various transitional metal oxides, such as HfO_2,[7] Al_2O_3,[8] $SrTiO_3$,[9] and so on. On the contrary, the TS is a type of volatile behavior with an S-shape I-V curve that works in limited voltage range between two critical values called the holding voltage (V_H) and threshold voltage (V_{TH}). Differing from nonvolatile MS, LRS in TS will switch back to HRS as applied bias is below V_H, that is, HRS retains below V_H and only LRS is displayed above V_{TH}. Many investigations have demonstrated the excellent selector function of TS to suppress the sneak problem of high-density crossbar arrays as connected with RRAM in series [10-13]. Even conversion between MS and TS under the suitable external excitation was also reported.[5, 6, 14, 15]

Lately, an important nonlinear carrier-transport phenomenon-negative differential resistance (NDR), referring to a decrease in current with increasing

voltage or vice versa, has been discovered accompanying with various RS, such as unipolar RS on $Ag/SiO_2/Pt$ device,[16] multilevel RS on $Pt/BaSrTiO_3/SrTiO_3$:Nb device,[17] bipolar RS on Ag/ZnO/Zn device[18] and flexible organic memristive memory [19]. However, the origin of NDR in RS is controversial. Discharging electrons from metal nanocrystals, charge storage processes between interfaces, separation of oxygen vacancies and trapped electrons, and different work functions of materials have been proposed to contribute to NDR. Furthermore, the compliance current (I_{cc}) is a vital parameter for RRAM to understand and manipulate RS, but the effects of I_{cc} on NDR are still insufficient. In this work, conversion from bidirectional TS to MS were achieved on $Ag/HfO_x/Pt$ device through controlling I_{cc}. NDR can be observed in TS with I_{cc} lower than 800μA. The dependence of NDR on I_{cc} was also investigated by manipulating TS via I_{cc}. The phenomena can be elucidated in the view of conductive filaments model as well as nanocapacitor effects originated from filament gap.

2. Experimental section

The HfO_x films were directly deposited on the available $Pt/TiO_2/SiO_2/Si$ substrates by atomic layer deposition (ALD) system with tetrakis-(dimethylamido)-hafnium ($Hf(NMe_2)_4$) as the precursor source, purified water as the oxygen source and purified nitrogen as the carrier gas. For one typical growth cycle, $Hf(NMe_2)_4/N_2/H_2O/N_2$ with the exposure time of 0.15s/15s/0.15s/15s was performed, and 250 cycles were carried out to deposit HfO_x thin film with thickness of ~30nm. To fabricate $Ag/HfO_x/Pt$ devices, the top Ag electrodes were subsequently

deposited on the surface of as-fabricated HfO_x films through a shadow mask. The diameter and the thickness of the top electrodes are ~100μm and ~100nm, respectively. The schematic diagram of Ag/HfO_x/Pt devices was illustrated as inset of **Fig. 1(a).** The electrical performances of device were characterized by scanning the current-voltage (I-V) curves using a Keithley 4200 semiconductor parameter analyzer at room temperature. The voltage step is fixed to be 0.05V, and the collecting time for each data point is 0.1ms containing delay time and holding time. For all measurements, the bias voltage was applied on the bottom Pt electrodes, while the top Ag electrodes were grounded all along.

3. Results and discussion

A pristine Ag/HfO_x/Pt device stays HRS. To get the switching effects, an electroforming process was generally needed. It has been reported that the resistive switching performances are well dependent on the electroforming process like polarity, sequence of I_{cc}.[20-21] Also, double and asymmetric two-step electroforming are reported to be beneficial to stabilize the resistive switching.[7] Here, an incomplete electroforming process with I_{cc} of 10μA was applied by performing a positive sweeping 0 ~+8V. As **Fig. 1(a)** indicates, the current is far lower than 10μA and there is no abrupt current rise in this process. After that, the sweeping setup of 0V→−0.4V→0V→0.4V→0V was subsequently performed. **Fig. 1(b)** exhibits I-V curves with I_{cc} of 10μA in semi-logarithmic scale. It is evident that a Set switching from HRS to LRS firstly occurs at a negative threshold voltage (V_{TH}^-) ~ -0.25V in the following sweeping from 0V to -0.4V, and a Reset switching from LRS to HRS

appears at negative hold voltage (V_H^-) ~-0.12V as voltage reverted back from -0.4V to 0V. Similarly, the nearly symmetric Set and Reset switching occur in the positive bias branch with a positive threshold voltage (V_{TH}^+) ~ 0.22V and hold voltage (V_H^+) ~ 0.05V, respectively. It is worthy of noting that when voltage scanned backward from +0.4V/-0.4V to 0V, NDR occurred obviously once voltage is below V_H in both negative and positive bias branches. **Fig. 1(c) and Fig. 1(d)** display the typical I-V and dynamic conductance (*dI/dV*)-*V* curves at linear scale where NDR appears. Whether the voltage sweeps from V_H^+ or V_H^- to 0V, current increases gradually, while dynamic conductance degrades. Similar NDR was achieved in all TS curves. Moreover, it is of significant importance to emphasize that negative current was detected in positive NDR bias but positive current emerges in negative NDR bias.

In spite of facts that conversion between TS and MS depending on I_{cc} as well as NDR have been widely reported,[16-18, 22-24] I_{cc}-dependent NDR is still undiscovered. For this sake, the bidirectional TS with NDR was further purchased and systematically compared under various I_{cc} of 1μA, 10μA, 20μA, 50μA, 100μA, 150μA, 500μA and 800μA. **Fig. 2(a)** and **2(b)** show some typical I-V curves and corresponding evolution of switching voltages with I_{cc}, including V_H^+, V_H^-, V_{TH}^+ and V_{TH}^-. As **Fig. 2(a)** indicates, Ag/HfO_x/Pt device evidently manifests the bidirectional TS with NDR as I_{cc} is below 800μA. With enhancing I_{cc} from 1μA to 800μA, all threshold voltages V_{TH}^+ and V_{TH}^- evolve towards the lower value (**Fig. 2(b)**). Although the holding voltage V_H^+ and V_H^- increase slightly in small I_{cc}, both descend eventually as I_{cc} rises up. Meanwhile, the readout windows, defined as the voltage gap

between V_H and V_{TH}, drop gradually with increasing I_{cc} (Inset in **Fig. 2(b)**). However, TS of Ag/HfO_x/Pt device becomes unstable when I_{cc} is over 800μA, and converses to MS as I_{cc} is larger than 1mA. **Fig. 2(c)** displays I-V curves within continuous 600 cycles with I_{cc} of 5mA, featuring with typical nonvolatile MS. The corresponding evolution of Reset/Set voltages and resistance at 0.05V, shown in **Fig. 2(d),** indicate that the uniform RS can be obtained on Ag/HfO_x/Pt device in a suitable I_{cc}. Interestingly, NDR which emerges in all bidirectional TS, cannot be observed in MS performances.

As result of the evolution of TS with I_{cc}, the unique dependence of NDR on I_{cc} can be probably explored. During the voltage scanning, the voltage step is fixed to be 0.05V, and the collecting time for each data point is calculated to be 0.1ms containing delay time and holding time. Therefore, *dI/dV* as a function of time in NDR region was derived from various I_{cc} to further understand the effects of I_{cc} on NDR. **Fig. 3(a)~3(d)** illustrate the typical *dI/dV-t* plots with I_{cc} of 1μA, 10μA, 20μA, 50μA, respectively, which were derived from negative NDR bias region. The black lines are fitting results with an exponential relaxation equation $dI/dV = A\,exp\left(-\frac{t}{\tau}\right)$, where t is the relaxation time, A refers to the initial value of *dI/dV*, and τ is the relaxation time constant. Obviously, the experimental data is in good accordance with the fitting results, which means *dI/dV-t* plot can be expressed by a capacitor-like relaxation equation. It also suggests that NDR in TS here is possibly originated from capacitive effects. **Fig. 3(e)** displays the evolution of parameter τ with investigated I_{cc} from 1μA to 800μA. Interestingly, there are two stages for variation of τ with I_{cc}. τ decreases

slightly from ~0.18ms to ~0.16ms as I_{cc} changes from 1μA to 50μA but with small deviation in each I_{cc}. Then, τ rises dramatically to be ~0.26ms with large deviation as I_{cc} exceeds 100μA. It implies the deteriorated uniformity of TS on Ag/HfO_x/Pt device in large I_{cc}.

Many investigations have directly observed growth and annihilation of Ag nanofilaments via electrochemical redox process in Ag-based programmable metallization cells that causes Set and Reset switching in MS.[25, 26] The tiny Ag nanofilaments, especially in a low I_{cc}, are not stable due to Rayleigh instability. Therefore, the tiny nanofilaments will be dissolved spontaneously under surface energy as well as the diffusion into matrix due to the concentration gradient and thermal effects,[26, 27] resulting in the volatile TS accordingly. For both MS and TS, I_{cc} plays a particularly important role in manipulating nanofilaments morphology. [16,18, 25-27] Therefore, on basis of abovementioned analysis, the I_{cc}-dependent NDR in this work can be understood from viewpoint of the evolution of Ag conductive nanofilaments coupling with the capacitive effects of nanocapacitor resulted from nanofilaments gap. **Fig. 4** schematically illustrates the overall evolution of Ag nanofilaments and nanocapacitor as well as the corresponding equivalent circuits in TS and MS. Initially, incomplete electroforming did not switch Ag/HfO_x/Pt device to LRS. As the negative bias was applied on the Pt electrode, Ag nanofilaments grew along the old one and switched device to LRS as bias came to V_{TH}^- (**Fig. 4(a)**). But tiny nanofilaments formed due to the limitation of low I_{cc}. The tiny Ag nanofilaments can be equivalently considered as a resistance and are unstable in nano scale, which

dissolved spontaneously under surface energy, resulting in switching back to HRS at V_H^- (**Fig. 4(b)**). Then, the residual nanofilaments in HfO_x films were disconnected with nanogap. Due to high conductivity of Ag nanofilaments, the overall device resembles nanocapacitor with two resistances in series, the equivalent circuit is shown in right side of **Fig. 4(b).** As the applied bias was below V_H^-, the nanocapacitor discharged, enhancing current of circuit, namely NDR. It also created the reverse current owing to the opposite electric field direction between nanocapacitor and applied bias. Similar processes occurred in the positive bias region, as shown in **Fig. 4(c) and 4(d).**

According to the model of a plane-parallel capacitor, the capacitance (C) can be expressed as $C = \frac{\varepsilon S}{4\pi k d}$, where ε is dielectric constant of dielectrics, S is area of parallel conductive nanofilaments cross sectional area, k is electrostatic constant, d is gap between counter nanofilaments. As mentioned, it is the discharging processes of nanocapacitor as bias is below hold voltage (V_H) that generates NDR phenomenon in Ag/HfO_x/Pt device and reverse current in the circuit. This discharging current of nanocapacitor can be characterized by equation of $I_t = I_s \exp\left(-\frac{t}{\tau}\right)$, where I_s is saturate current of pristine nanocapacitor. τ is the relaxation time constant referring to RC, where R is resistance value of residual nanofilaments. So, dI is also exponential function with time, but dV is constant due to the fixed voltage steps in measurement, which results in exponential *dI/dV-t* plot. And the relaxation time constant τ correlates with RC, where both R and C vary with I_{cc}. As I_{cc} increases from 1μA to 50μA, R decreases because of robust nanofilaments, leading to the

lower τ. However, S widens and d shortens as result of growth of nanofilaments under larger I_{cc}. Both can cause the larger C, resulting in dramatical enhancement of τ accordingly, shown as **Fig. 3(e)**. As I_{cc} further increases, the Ag nanoparticles inside filaments can further grow and connect with each other eventually to form continuous nanofilaments, which require more surface energy to dissolve due to large diameter. It causes disappearance of TS and dominance of MS, in which reversible formation and rupture of the robust nanofilaments results in Set and Reset switching, shown as **Fig. 4(e)** and **4(f)**. However, NDR in TS disappears in MS. This is reasonably believed that the slight current discharged from nanocapacitor is negligible compared with that of LRS in MS. In any case, the I_{cc}-dependent NDR as well as conversion between TS and MS on Ag/HfO_x/Pt resistive memory device indicate its potential application as a multifunctional electronic device.

4. Conclusions

In summary, we investigated the dependence of NDR on I_{cc} based on Ag/HfO_x/Pt resistive memory device. In addition to bipolar memory switching in large I_{cc}, the as-fabricated device exhibit bidirectional threshold switching with NDR in low I_{cc}. This NDR is significantly dependent on I_{cc}, and the dynamic conductance *dI/dV-t* plot in NDR is good accordance to the capacitor-like relaxation equation. These phenomena were attentively elucidated from viewpoint of filaments evolution controlled by I_{cc} as well as nanocapacitor effects resulted from filaments gap.

Conflicts of interest

There are no conflicts to declare.

Acknowledgements

The authors gratefully acknowledge support from the National Nature Science Foundation of China (61674059), the Science and Technology Planning Project of Guangdong Province (2015A010103012), the Science and Technology Planning Project of Guangzhou City (201804010399), and the Innovative Project of Education Department of Guangdong Province (2017KTSCX050).

References

[1] Waser R, Aono M (2009) Nanoionics-based resistive switching memories. Nanoscience and Technology: A Collection of Reviews from Nature Journals 158–165. https://doi.org/10.1142/9789814287005_0016

[2] Yang JJ, Pickett MD, Li X, et al (2008) Memristive switching mechanism for metal/oxide/metal nanodevices. Nature Nanotechnology 3:429–433. https://doi.org/10.1038/nnano.2008.160

[3] Kagan CR, Lifshitz E, Sargent EH, Talapin D V. (2016) Building devices from colloidal quantum dots. Science 353:. https://doi.org/10.1126/science.aac5523

[4] Watanabe Y, Bednorz JG, Bietsch A, et al (2001) Current-driven insulator-conductor transition and nonvolatile memory in chromium-doped $SrTiO_3$ single crystals. Applied Physics Letters 78:3738–3740. https://doi.org/10.1063/1.1377617

[5] Chang SH, Lee JS, Chae SC, et al (2009) Occurrence of both unipolar memory and threshold resistance switching in a NiO film. Physical Review Letters 102:1–4. https://doi.org/10.1103/PhysRevLett.102.026801

[6] Peng HY, Li YF, Lin WN, et al (2012) Deterministic conversion between memory and threshold resistive switching via tuning the strong electron correlation. Scientific Reports 2:1–6. https://doi.org/10.1038/srep00442

[7] Chen X, Hu W, Li Y, et al (2016) Complementary resistive switching behaviors evolved from bipolar TiN/HfO_2/Pt device. Applied Physics Letters 10

8:. https://doi.org/10.1063/1.4941287

[8] Hubbard WA, Kerelsky A, Jasmin G, et al (2015) Nanofilament Formation and Regeneration during Cu/Al_2O_3 Resistive Memory Switching. Nano Lette rs 15:3983–3987. https://doi.org/10.1021/acs.nanolett.5b00901

[9] Mikheev E, Hoskins BD, Strukov DB, Stemmer S (2014) Resistive switchi ng and its suppression in Pt/Nb:$SrTiO_3$ junctions. Nature Communications 5: . https://doi.org/10.1038/ncomms4990

[10] Liu D, Cheng H, Wang G, et al (2013) Diode-like volatile resistive switc hing properties in amorphous Sr-doped $LaMnO_3$ thin films under lower cur rent compliance. Journal of Applied Physics 114:1–6. https://doi.org/10.1063/ 1.4826362

[11] Liu T, Verma M, Kang Y, Orlowski M (2012) Volatile resistive switching in Cu/TaO x/δ-Cu/Pt devices. Applied Physics Letters 101:2–6. https://doi.o rg/10.1063/1.4746276

[12] Chen W, Barnaby HJ, Kozicki MN (2016) Volatile and Non-Volatile Switc hing in Cu-SiO_2 Programmable Metallization Cells. IEEE Electron Device Letters 37:580–583. https://doi.org/10.1109/LED.2016.2540361

[13] Li Y, Yuan P, Fu L, et al (2015) Coexistence of diode-like volatile and multilevel nonvolatile resistive switching in a ZrO_2/TiO_2 stack structure. Na notechnology 26:. https://doi.org/10.1088/0957-4484/26/39/391001

[14] Qi J, Olmedo M, Zheng JG, Liu J (2013) Multimode resistive switching i n single ZnO nanoisland system. Scientific Reports 3:1–6. https://doi.org/10.

1038/srep02405

[15] Pan C, Ji Y, Xiao N, et al (2017) Coexistence of Grain-Boundaries-Assisted Bipolar and Threshold Resistive Switching in Multilayer Hexagonal Boron Nitride. Advanced Functional Materials 27:. https://doi.org/10.1002/adfm.201604811

[16] Sun H, Liu Q, Long S, et al (2014) Multilevel unipolar resistive switching with negative differential resistance effect in Ag/SiO2/Pt device. Journal of Applied Physics 116:1–6. https://doi.org/10.1063/1.4898807

[17] He J, Zhu J, Ma C, et al (2019) Negative differential resistance and multilevel resistive switching in $BaSrTiO_3$ films. Applied Physics Letters 115:1–6. https://doi.org/10.1063/1.5113883

[18] Kadhim MS, Yang F, Sun B, et al (2018) A resistive switching memory device with a negative differential resistance at room temperature. Applied Physics Letters 113:1–6. https://doi.org/10.1063/1.5037191

[19] Zhu S, Sun B, Ranjan S, et al (2019) Mechanism analysis of a flexible organic memristive memory with capacitance effect and negative differential resistance state. APL Materials 7:. https://doi.org/10.1063/1.5100019

[20] Chen X, Hu W, Wu S, Bao D (2014) Stabilizing resistive switching performances of TiN/MgZnO/ZnO/Pt heterostructure memory devices by programming the proper compliance current. Applied Physics Letters 104:1–5. https://doi.org/10.1063/1.4863744

[21] Li Y, Pan X, Zhang Y, Chen X (2015) Write-Once-Read-Many-Times and

Bipolar Resistive Switching Characteristics of TiN/HfO_2/Pt Devices Dependent on the Electroforming Polarity. IEEE Electron Device Letters 36:1149–1152. https://doi.org/10.1109/LED.2015.2477421

[22] Pickett MD, Borghetti J, Yang JJ, et al (2011) Coexistence of memristance and negative differential resistance in a nanoscale metal-oxide-metal system. Advanced Materials 23:1730–1733. https://doi.org/10.1002/adma.201004497

[23] Zhou G, Duan S, Li P, et al (2018) Coexistence of Negative Differential Resistance and Resistive Switching Memory at Room Temperature in TiOx Modulated by Moisture. Advanced Electronic Materials 4:1700567. https://doi.org/10.1002/aelm.201700567

[24] Du G, Li H, Mao Q, Ji Z (2016) Controllable volatile to nonvolatile resistive switching conversion and conductive filaments engineering in Cu/ZrO_2/Pt devices. Journal of Physics D: Applied Physics 49:. https://doi.org/10.1088/0022-3727/49/44/445105

[25] Sun H, Liu Q, Li C, et al (2014) Direct Observation of Conversion Between Threshold Switching and Memory Switching Induced by Conductive Filament Morphology. Advanced Functional Materials 24:5679–5686. https://doi.org/10.1002/adfm.201401304

[26] Hsiung CP, Liao HW, Gan JY, et al (2010) Formation and instability of silver nanofilament in Ag-based programmable metallization cells. ACS Nano 4:5414–5420. https://doi.org/10.1021/nn1010667

[27] Yang JJ, Strukov DB, Stewart DR (2013) Memristive devices for computing. Nature Nanotechnology 8:13–24. https://doi.org/10.1038/nnano.2012.240

Figure Captions

Figure 1 **(a)** An incomplete electroforming process on Ag/HfO_x/Pt device. Inset shows schematic diagram of Ag/HfO_x/Pt device. **(b)** Typical I-V curves of bidirectional TS at I_{cc}=10μA. Typical I-V and derived *dI/dV-V* curves in NDR of positive **(c)** and negative **(d)** bias region with I_{cc}=10μA.

Figure 2 **(a)** Bidirectional TS characteristic curves at I_{cc} of 1μA, 10μA, 150μA, 800μA. **(b)** Evolution of V_H^+, V_H^-, V_{TH}^+ and V_{TH}^- with I_{cc}. Inset shows the corresponding evolution of readout windows. **(c)** Typical I-V curves of MS with I_{cc}=5 mA. **(d)** Evolution of resistance at 0.05V and switching voltages for MS within 600 cycles.

Figure 3 *dI/dV-t* plots and fitting results with relaxation equation for NDR with various I_{cc}: **(a)** 1μA, **(b)** 10μA **(c)** 20μA and **(d)** 50μA. **(e)** Evolution of relaxation time constant τ with I_{cc}.

Figure 4 Schematic diagrams of the model corresponding to the various states of device. After a low I_{cc} electroforming, tiny conductive nanofilaments formed and the device performs as TS: **(a)** Negative ON states. **(b)** Negative OFF states. **(c)** Positive OFF states. **(d)** Positive ON states. The device performs as MS in large I_{cc}: **(e)** OFF states. **(f)** ON states.

Figures

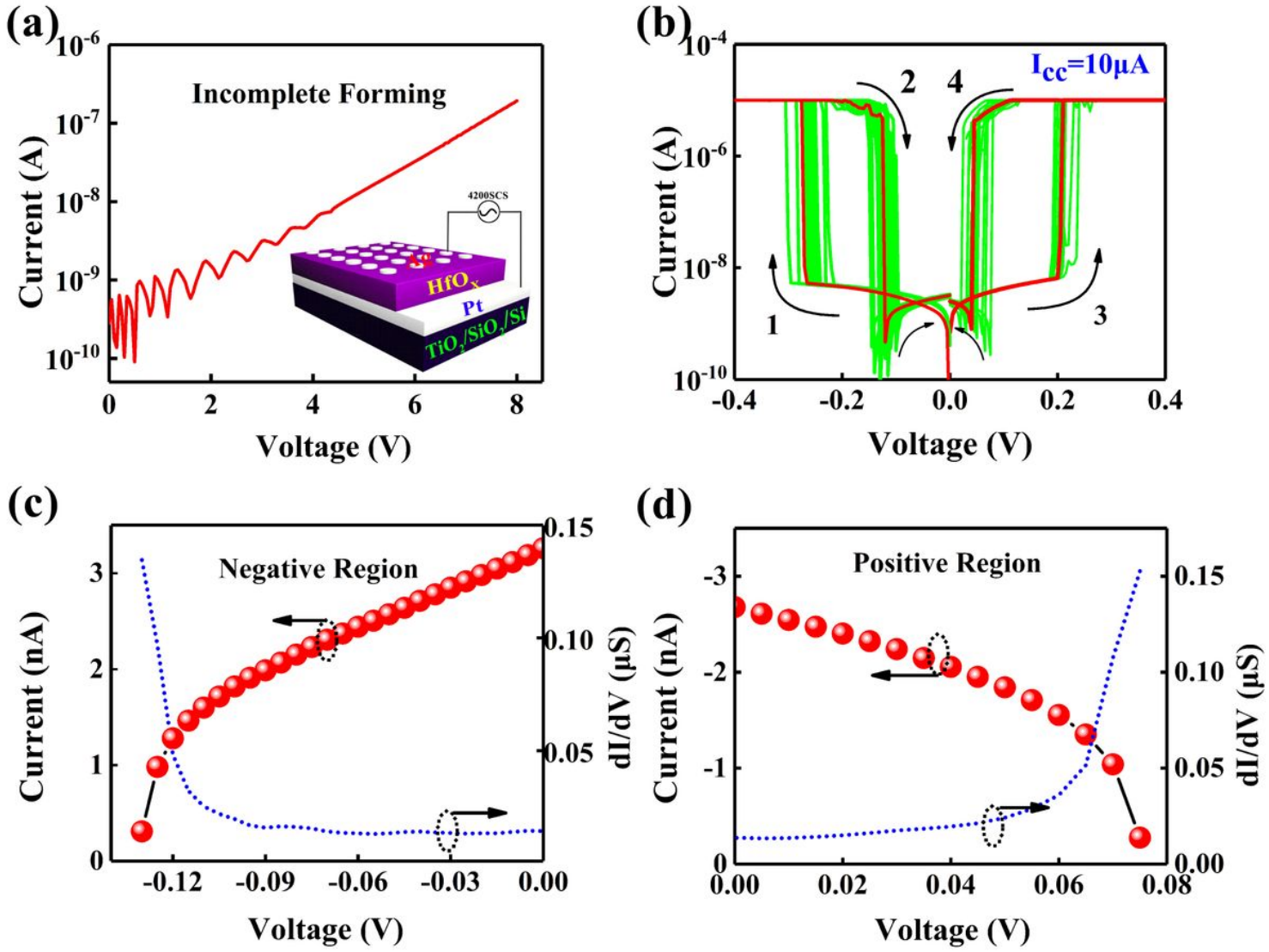

Figure 1

(a) An incomplete electroforming process on Ag/HfOx/Pt device. Inset shows schematic diagram of Ag/HfOx/Pt device. (b) Typical I V curves of bidirectional TS at Icc=10μA. Typical I V and derived dI/dV V curves in NDR of positive (c) and negative (d) bias region with Icc=10μA.

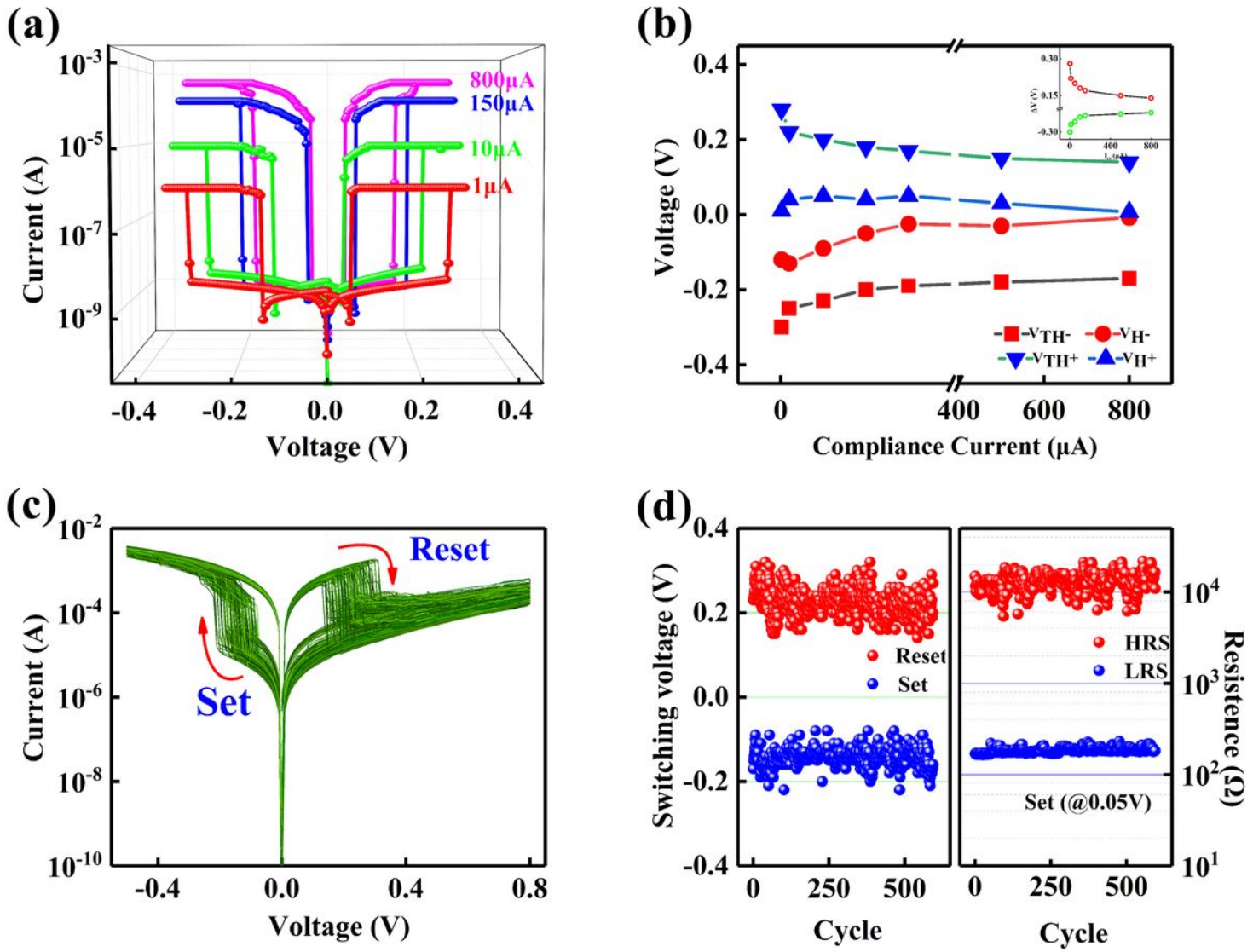

Figure 2

(a) Bidirectional TS characteristic curves at Icc of 1μA, 10μA, 150μA, 800μA. (b) Evolution of VH+, VH–, VTH+ and VTH with Icc. Inset shows the corresponding evolution of readout windows. (c) Typical I V curves of MS with Icc=5 mA. (d) Evolution of resistance at 0.05V and switching voltages for MS within 600 cycles.

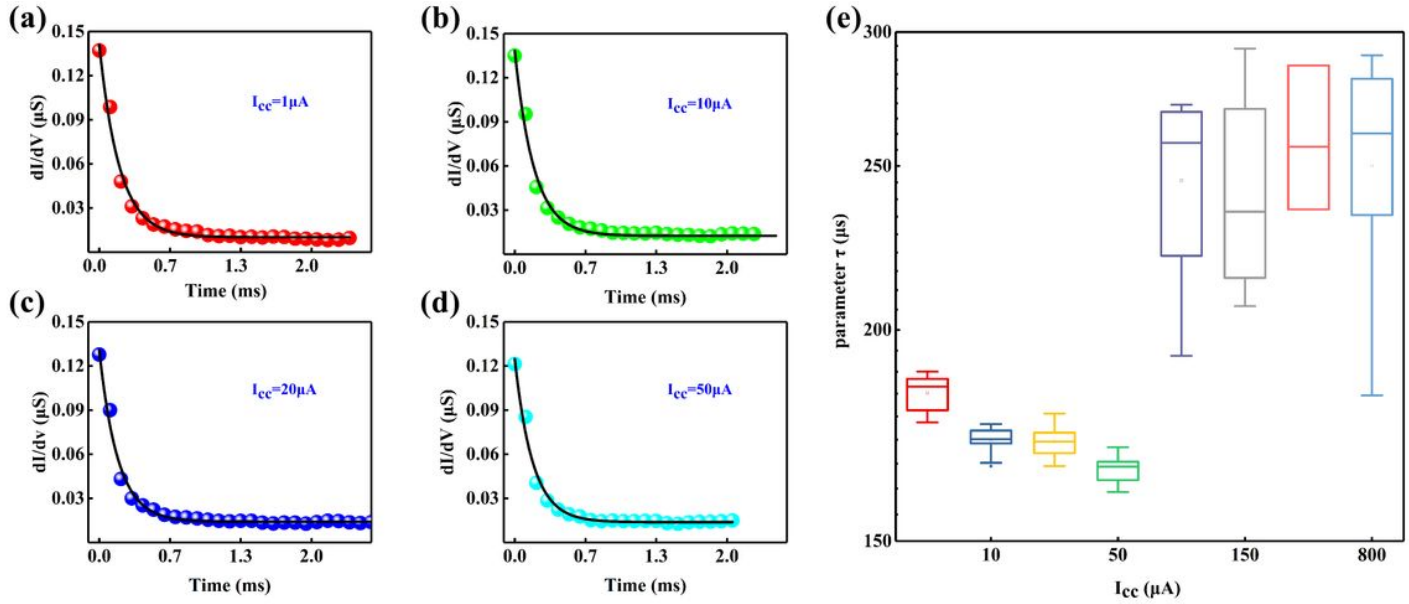

Figure 3

dI/dV t plots and fitting results with relaxation equation for NDR with various Icc: (a) 1μA, (b) 10μA (c) 20μA and (d) 50μA. (e) Evolution of relaxation time constant ⍰ with Icc.

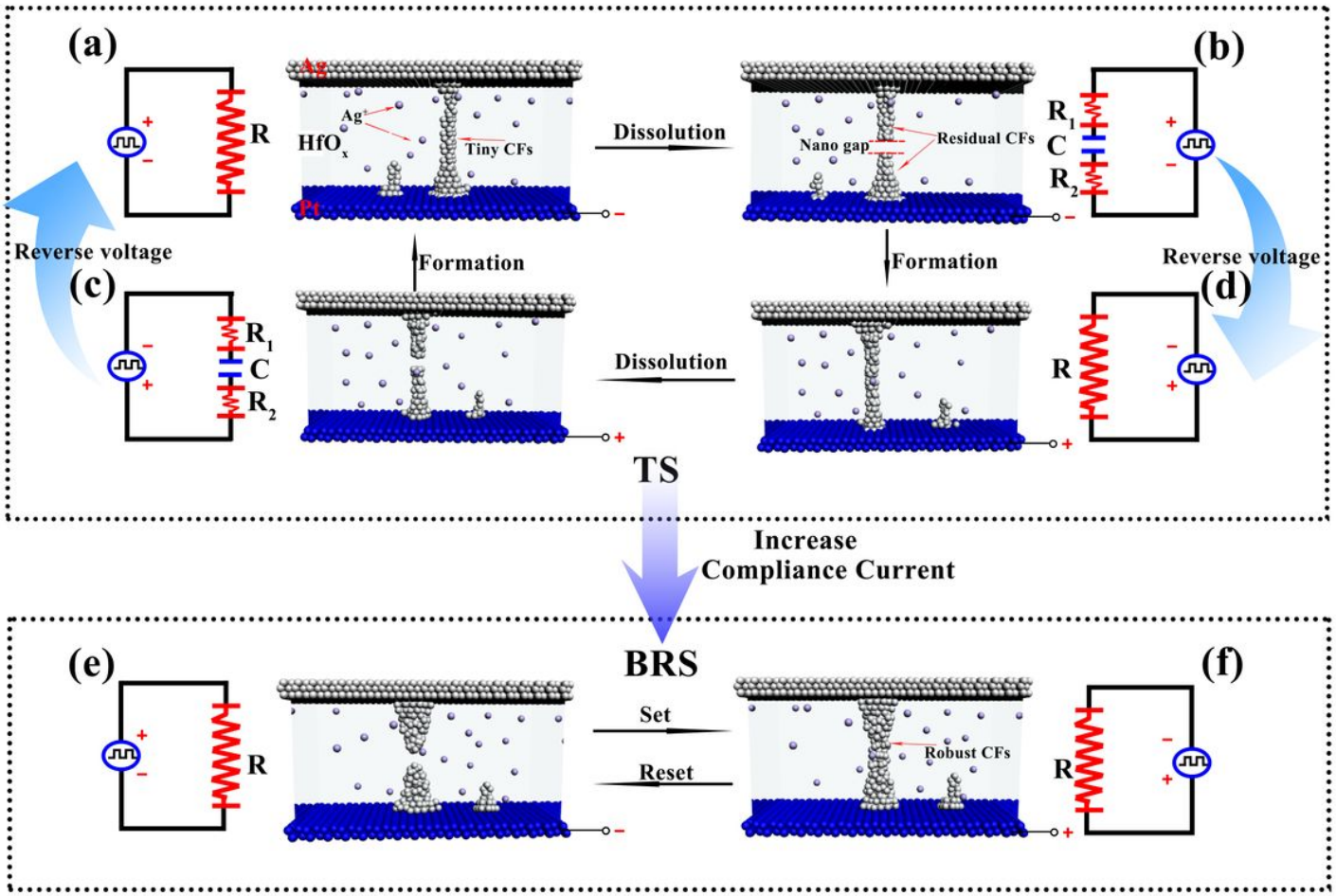

Figure 4

Schematic diagrams of the model corresponding to the various states of device. After a low Icc electroforming, tiny conductive nanofilaments formed and the device performs as TS: (a) Negative ON states. (b) Negative OFF states. (c) Positive OFF states. (d) Positive ON states. The device performs as MS in large Icc: (e) OFF states. (f) ON states.